Green light from red-emitting nanocrystals: broadband, low threshold lasing from colloidal quantum shells in optical nanocavities

Kehui Zhao¹, Xiaohe Zhou¹, Xi Li,², Jiyoung Moon², James Cassidy⁴, Dulanjan Harankahage⁴, Zhongjian Hu⁵, Stephen Savoy⁵, Qing Gu^{2,3}, Mikhail Zamkov⁴ and Anton V. Malko¹

¹Department of Physics, The University of Texas at Dallas, Richardson, Texas 75080

²Department of Electrical and Computer Engineering, North Carolina State University, Raleigh, North Carolina 27695, USA

³Department of Physics, North Carolina State University, Raleigh, North Carolina 27695, USA

⁴The Center for Photochemical Sciences and Department of Physics, Bowling Green State University, Bowling Green, Ohio 43403.

⁵Nanohmics Inc, 6201 E. Oltorf, Suite 400, Austin, TX, 78741, USA

Corresponding author: anton.malko@utdallas.edu

Spherical semiconductor nanoplatelets, known as quantum shells (QSs), have captured significant interest for their strong suppression of Auger recombination, which leads to long multi-exciton lifetimes and wide optical gain bandwidth. Yet, the realization of unique benefits associated with the multi-exciton lasing regime using a suitably designed photonic cavity remains elusive. Here, we demonstrate broadly tunable lasing from close-packed films of CdS/CdSe/CdS QSs deposited over nanopillar arrays on Si substrates. Wide spectral tuning of the stimulated emission in QSs with a fixed band gap value was achieved by engaging single exciton (λ_X ~634 nm), biexciton (λ_B_X ~625 nm), and multiple exciton (λ_M_X ~615-565 nm) transitions. The ensemble-averaged gain threshold of < N>~2.6 electron-hole pairs per QS particle and the record-low photonic cavity fluence threshold of $< 4 \mu J/cm^2$ were attributed to Auger suppression. The tuning of the lasing emission closely aligns with our model predictions, achieved by varying the array period while preserving mode confinement and quality (Q) factors. These results mark a notable step toward the development of colloidal nanocrystal lasers.

Introduction and motivation

The integration of electrically pumped lasers and optical amplifiers with existing silicon-based semiconductor frameworks is a significant challenge in the field of optoelectronics. Current strategies involve complex processes like wafer-bonding or off-chip III-V laser integration into Si microstructures, which increases both the complexity and production costs of these devices. Consequently, the use of low-cost solution-processed materials for the development of lasers/amplifiers holds promise for numerous applications. This method could enable large-scale, on-chip integration of both photonic and electronic components, catering to the growing demand for diverse photonic quantum information processing architectures. Moreover, solution-processable lasing devices could play a vital role in a range of sectors, including medical and wearable diagnostic technologies. As

Colloidal semiconductor nanocrystals (NCs) hold a unique position among solution-processable gain media. ^{6,7,8,9} These nanomaterials effectively blend well-known benefits of inorganic semiconductors with the chemical flexibility of molecular structures, facilitating their integration into photonic and electronic systems without the need for lattice matching or complex vacuum-based fabrication methods. Additionally, these NCs can be synthesized in a diverse array of sizes, shapes, and compositions, enabling emission bands spanning ultraviolet (UV) to infrared (IR). ^{10,11} This versatility is further enhanced by the quantum confinement achievable through various degrees of size quantization in different dimensional structures, such as 0D nanocrystal quantum dots (QDs)¹², 1D quantum nanorods (NRs)¹³, and 2D quantum wells (QWs) or nanoplatelets (NPLs). ^{14,15}

The employment of colloidal NCs for lasing applications is strongly impeded by the non-radiative Auger recombination processes affecting optically active multiple charge carriers like biexcitons (BX) and multiexcitons (MX). Recent efforts in developing various nanocrystal structures and geometries have focused on mitigating Auger effects, particularly with stepwise or continuous composition-graded colloidal nanocrystal QDs 18,19 and flat NPLs. The former, noted for their prolonged radiative BX lifetimes, have been prominently featured in recent demonstrations of continuous wave (CW) lasing 1 and electrical injection. The latter, while offering large oscillator strength 4 and extremely narrow emission linewidth, have shorter BX emission lifetimes, which poses challenges for optical gain development and has limited their ability to achieve low lasing thresholds in optical microcavity configurations.

In our recent work, we have advanced the scope of potential solutions and addressed issues concerning multiexciton lifetimes by creating a novel type of quasi-two-dimensional NC geometry. These so-called quantum shells (QS) represent a spherical QW structure comprising a CdSe quantum-confined spherical shell sandwiched between bulk-size CdS core and CdS outer layers. ^{26,27,28,29,30,31,32} Like nanoplatelets, quantum shells provide carrier confinement in only one dimension but with repulsive rather than attractive interactions between multiple excitons. This repulsion between excitons results in reduced carrier overlap, subsequently leading to a dramatically decreased rate of Auger recombination to a point where radiative emission from biexcitons approaches 100%.³³

To take advantage of efficient gain media, it is essential to employ a suitable optical cavity. Fortunately, colloidal nanocrystals can be incorporated into a far wider array of optical cavities compared to their epitaxial semiconductor counterparts. To date, colloidal nanoparticles have been

included in the various microcavities including microring/sphere cavities, 34,35 vertical surface-emitting laser (VCSEL) with distributed Bragg reflector (DBR) mirrors 36 , Fabry-Perot cavity, 37 distributed feedback (DFB) cavities 38,39 and photonic crystal (PhC) cavities. 40,41,42 Among them, DFB optical resonators in the form of nanopillar PhC arrays present a number of practical advantages, such as tunabilty of the resonant wavelength by manipulation of the array period, comparatively high quality (Q) factors and small mode localization volumes and easy lithographic fabrication methods. Additionally, they would potentially decouple electrical injection (horizontally) and optical emission pathways (vertically) while allowing for dense NQD packing.

Integrating colloidal nanocrystals into a photonic crystal cavity presents unique challenges. First, achieving a uniform dispersion of nanocrystals within the cavity without altering their intrinsic optical properties is a major hurdle, necessitating proper surface chemistry techniques to ensure compatibility and stability. Second, the precise engineering of the photonic crystal structure to match the emission wavelength of nanocrystals is critical for achieving efficient lasing. This requires accurate control over the lattice parameters within the photonic crystal. Finally, it is important to maintain the quantum efficiency of nanocrystals within the complex environment of the photonic crystal.

In the current study, we demonstrate broadband, low-threshold lasing emission from a closed-packed layer of CdS/CdSe/CdS spherical QSs incorporated within SiO₂ PhC nanopillar arrays etched on Si substrates. The suppression of multi-exciton Auger recombination in QSs enabled us to achieve a significant spectral tuning of the lasing emission from QSs with a fixed size. Together with high quality factors and minimal optical losses of the nanopillar cavity, we recorded a remarkably low threshold pump fluence of approximately $w \sim 4 \,\mu\text{J/cm}^2$, near the record low for

colloidal nanomaterials in the optical cavity configuration. The investigation of eigenfrequencies using the finite element method (FEM) facilitated the identification of eigenmodes, while frequency domain analysis was employed to acquire the transmission spectrum and cavity factors of multiple Fano resonances close to the lasing emission wavelengths, with Q~6000. Lasing threshold gain values were modelled to be in the range of g ~ 40 - 80 cm⁻¹, demonstrating a reduction by an order of magnitude relative to a planar film configuration and underscoring the advantages of the photonic optical nanocavity.

Results and Discussion

In our prior works, we have compared amplified spontaneous emission (ASE) characteristics across CdS/CdSe/CdS QSs with different CdSe quantum-well volumes.^{32,33} In the present study, we have chosen QSs with the 6-nm CdS core size as a representative example of quantum shells showing broad-band gain from X, BX and MX transitions across the 570 to 630 nm range. High resolution transmission electron microscopy (TEM) image of an individual quantum shell, shown in **Figures 1(a) and S5**, exhibits three contrasted domains, corresponding to CdS core, CdSe

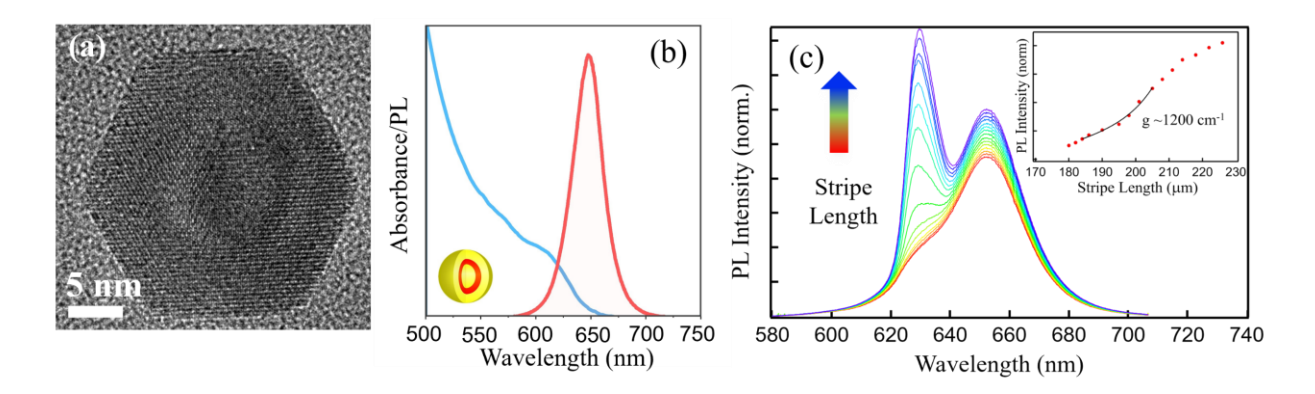


Figure 1. (a) High resolution TEM image of an individual 6 -nm core QS. (b) Linear absorption and PL emission spectra of the 6 nm CdSe/CdS/CdSe quantum shells in solution. (c) Room temperature PL intensity of a QS thin film at various stripe lengths of the excitation spot. Inset: Integrated intensity of the ASE vs. stripe length.

quantum-well layer, and CdS surface-barrier shell. The hexagonal shape of these nanocrystals suggests a thermodynamically evolved morphology, achieved by high-temperature annealing. Details of the colloidal QS synthesis are provided in the Supplementary Information (SI) and can also be found in Refs. [32, 33]. Linear optical absorption and PL emission of 6-nm core QSs in solution are demonstrated in Figure 1(b), illustrating a good size uniformity and emission profile. The observed full width half maximum (FWHM) of the bulk emission profile is approximately 96 meV, on par with that of high-quality core-shell CdSe/CdS nanocrystals. A relatively narrow linewidth of our sample is likewise corroborated by a low particle size dispersion, as seen in the TEM images (Figure S5). Figure 1(c) shows PL emission as a function of variable stripe length l of the excitation profile from a QS thin film drop-casted on a glass substrate. Schematics of the variable stripe configuration are shown in Figure S1. ASE develops at BX transition and exhibits superlinear growth, characteristic of the optical amplification. Modal gain (i.e. gain minus optical propagation losses) magnitude g reaches values g>1000 cm⁻¹ at high fluence, confirming the potential of this material for lasing applications. In addition, ASE develops at higher energy transitions (i.e. excited state biexciton, 1S(e)2S(h) and multiexcitons, 1P(e)1P(h)) at the increased excitation fluence, Figure S2.

Photonic crystal cavities in the form of SiO₂ nanopillar arrays on Si substates were formed with e-beam lithography followed by dry etching. These arrays feature dimensions of 100 x 100 μm and are spaced 500 μm apart. Nanopillar diameters and lattice periods were varied to finely adjust the resonance frequency of the PhC for different spectral regions in the optical gain (*i.e.* exciton, biexciton, multiexciton), as shown in **Figures S3** and **S4**. Details of the fabrication procedure are provided in the SI. The laser cavity was completed by spin-coating QSs on the entire sample that contains 24 PhC patterns with varying array periods (Λ). **Figure 2(a, b)** shows SEM and optical

images of the PhC arrays before and after QSs spin-casting. SEM image also indicates that spincoating results in close-packed QSs' layer with the depth at or exceeding the nanopillars' height. To match the PhC resonant wavelengths with various transitions within the gain bandwidth of the chosen QSs, the PhC arrays are designed with periods varying from $\Lambda=315$ nm to $\Lambda=365$ nm. The optical excitation schematics is illustrated in Figure 2(c). Each individual PhC array is optically pumped by 400 nm pulses from an amplified femtosecond laser coupled to the microscope objective. The excitation spot size is intentionally defocused using a short focal distance lens placed before the microscope to excite larger PhC surface area on each pattern, with an effective diameter $\phi = 50 \mu m$. The resulting pump fluences (w) range from $w < 1 \mu J/cm^2$ to $w \sim 200 \mu J/cm^2$ corresponding to the average QS excitonic population < N > ranging from $< N > \sim 0.67$ to $< N > \sim 130$ electron-hole (eh) pairs (see Figure S5 for more high-resolution QS TEM images and details and determination of QS's absorption cross-section). The PL emission is collected by the same objective and sent to a spectrometer equipped with a CCD camera for spectral analysis or to an avalanche photodiode (APD) for time-resolved lifetime analysis. Measurements were performed at both low (77 K) and room temperatures (RT) with the help of an optical cryostat mounted on

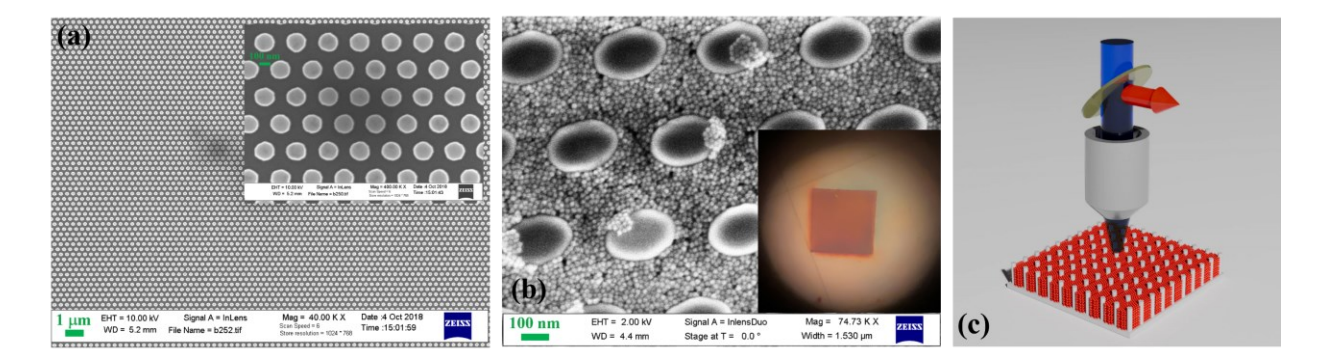


Figure 2. (a) SEM image of the PhC nanopillar array with period Λ =335 nm, scale bar – 1 μ m. Inset: magnified view of the array. Scale bar – 100 nm. (b) SEM image of the nanopillar array after QS spin-coating. Inset: optical image of the entire nanopillar array after spin coating. (c) Schematics of the excitation/collection geometry in the microscope system used in lasing experiments.

the microscope table.

Figure 3(a) illustrates the development of a sharp lasing mode with increasing excitation fluence in QSs with PL emission at approximately λ ~627 nm. These QSs were spin-coated on the PhC array with period Λ =355 nm and observed at 77 K. The onset of lasing is observed at a remarkably low fluence of about 4.2 µJ/cm², which is notably one of the lowest values recorded for colloidal nanocrystals in Distributed Feedback (DFB) configurations, ^{6,43} and it stands as the lowest fluence recorded for colloidal nanoparticles in photonic crystal cavities to date. 44 This particular fluence corresponds to an average excitonic population of $< N > \sim 2.6$, surpassing the previously established gain threshold identified in femtosecond pump-probe experiments. This transition corresponds to the BX emission state in these QSs. Near the threshold, lasing exhibits a single-mode behavior with a narrow fullwidth half maximum (FWHM) of $\delta\lambda \sim 0.5$ nm. Upon the increase in excitation fluence, the BX lasing mode broadens and shifts to the higher energy, in accordance with the power evolution of the TA gain profile. At fluences exceeding $w \sim 70 \text{ }\mu\text{J/cm}^2$, another set of emission modes appears at much higher emission energy (~570 nm), corresponding to lasing from MX transitions, Figure 3b. These findings, showcasing multi-exciton lasing, indicate a significant suppression of Auger recombination in quantum shells, which is on par with some of the top performing PhC lasers that utilize colloidal nanomaterials.

To analyze the lasing performance, we performed numerical simulations of the PhC using the finite element method (FEM) with the Wave Optics module in COMSOL Multiphysics. The eigenfrequency study was used to find the eigenmodes, and the frequency domain study was used to obtain the transmission spectrum and quality Q factor of the PhC cavity. **Figure 3(c,d)** illustrates the simulated optical transmission spectrum of the measured device of **Figure 3a**, where several transmission windows are observed in the wavelength range between 550 nm to 650 nm. A closer examination of the transverse magnetic (TM) mode transmission spectrum around the lasing

wavelength is presented in **Figure 3d**, featuring three Fano resonance peaks. The inset shows the electrical field distributions in the x-y plane for all three high Q factor modes under an oblique incidence of 0.5° . Notably, the mode resonant wavelength (transmission dips) align with the QS's gain spectrum, and the field maxima are located in the QS region. The mode distribution labeled "1" is the eigenmode with the highest Q factor, corresponding to the lowest threshold lasing mode. Modes "2" and "3", having lower Q factors, are located within 2 nm of the first lasing peak and are likely contributors to the broadening of this main lasing peak at higher excitation fluences, as

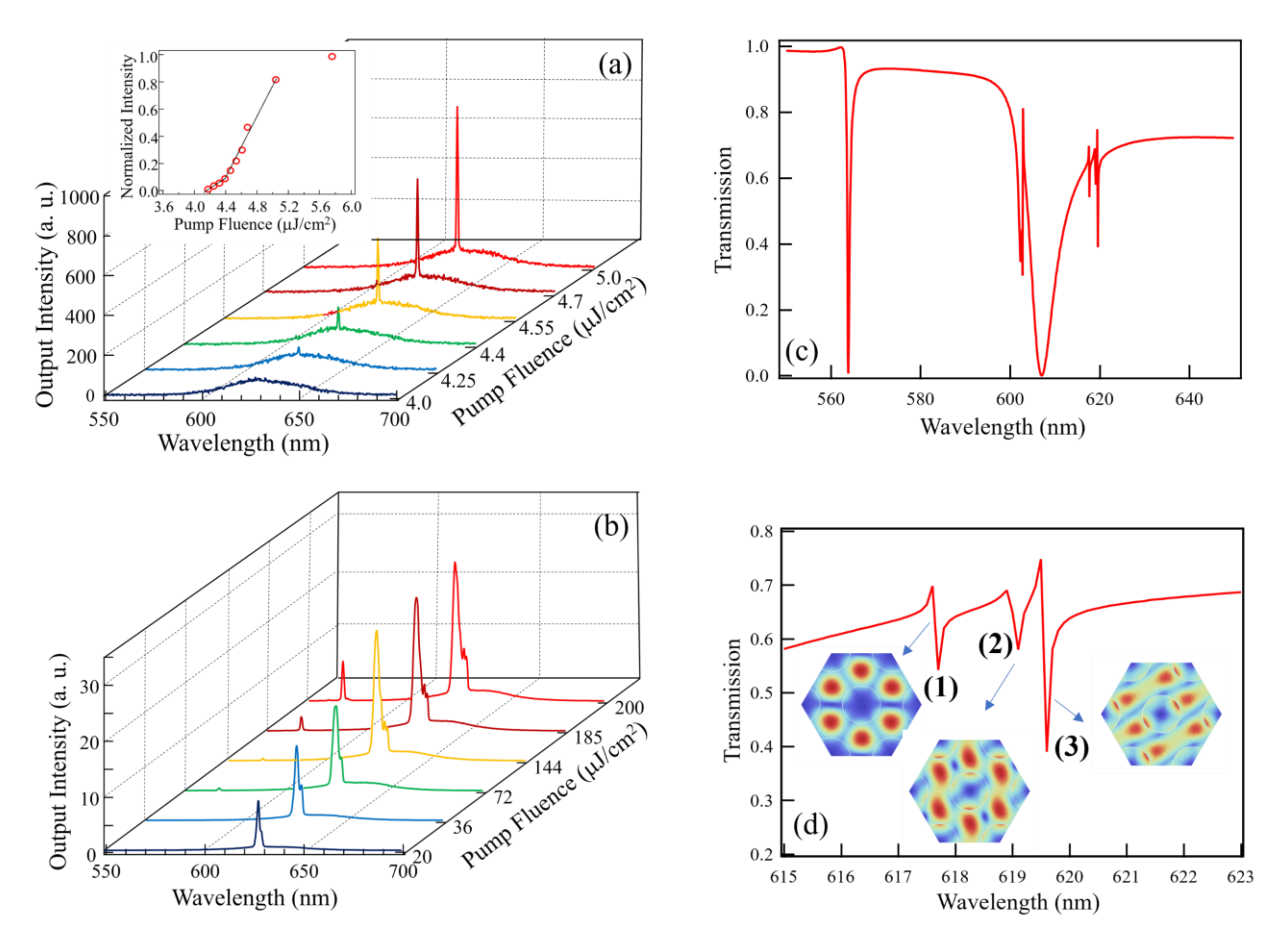


Figure 3. (a) Evolution of QS emission spectra in nanopillar PhC at 77K and low excitation fluences. Inset: Light-in versus light-out curve (LL curve) of the lasing mode (b) emission spectrum at high excitation fluences. (c) Simulated transmission spectrum of the PhC. (d) Zoomed-in view of the transmission spectrum around the measured lasing wavelength, showing three Fano resonance peaks near the resonance around 620 nm. Insets: mode profiles in the x-y plane at each transmission dip.

shown in **Figure 3b**. Additionally, a sharp transmission resonance at higher energy, correlating to lasing modes at approximately 565-570 nm, is observed within the MX gain transition.

The resonant wavelength in the nanopillar PhC cavity with a given height is influenced by several other parameters: the diameter (D), height (H) as well as the QS infilling factor within the array, which impacts the effective refractive index of the optical modes. The infilling factor, determined by the depth of QS packing between the nanopillars due to spin-coating, influences the observed differences between the lasing wavelengths and simulated resonances. These discrepancies likely result from variations in infilling factors, QS packing densities, and nanopillar diameters. Indeed, as demonstrated in **Figure S6**, the simulated lowest resonance wavelength is highly sensitive to both the QS layer thickness and the effective refractive index (n_{QS}) of the layer.

By changing the nanopillar lattice periods, we can tune the cavity resonant wavelength to align with different regions in the material's gain spectrum. In addition to BX lasing at 627 nm, **Figure 4** demonstrates several examples of wavelength dependent coupling of other excitonic transitions, starting from X at 635 nm (Λ =365 nm, **Figure 4a**) to excited state BX at 605 nm (Λ =335 nm, **Figure 4b**) to MX transitions at 568 nm (Λ =315 nm, **Figure 4c**). The last lasing wavelength is close to 1P_e-1P_h transitions. All spectra are taken at T=77 K to improve lasing thresholds. They gradually increase (**Figure 4d**), from $w \sim 4.2 \,\mu\text{J/cm}^2$ at BX transitions, to $w \sim 10 \,\mu\text{J/cm}^2$ for excited state BX and $w \sim 70 \,\mu\text{J/cm}^2$ for MX transitions. It is also evident that nanopillar cavity provides strong suppression of emission outside of the resonant modes, supporting single mode performance. Indeed, the BX emission line at 627 nm couples to the resonant mode of the cavity with Λ =365 nm, **Figure 3a** while the same emission wavelength is not coupled to the nanopillar array with Λ =335 nm, **Figure 4b** and is simply seen as a broadband ASE-type emission. The cavity

with the largest period only allows coupling of the emission at $\lambda \sim 634$ nm located at the lower portion of the gain profile for X emission, thus leading to higher threshold values, **Figure 4d**. We also recorded lasing emission at room temperature, **Figure 4e** for different array periods. While lasing thresholds are observed to be higher, the positions of lasing wavelengths may be directly compared to the simulated resonances, unimpeded by shifts of the optical gain regions, bandgap renormalization at low temperatures and possible reconfigurations of the nanopillar array dimensions. The simulated and experimental results agree well, again with some differences

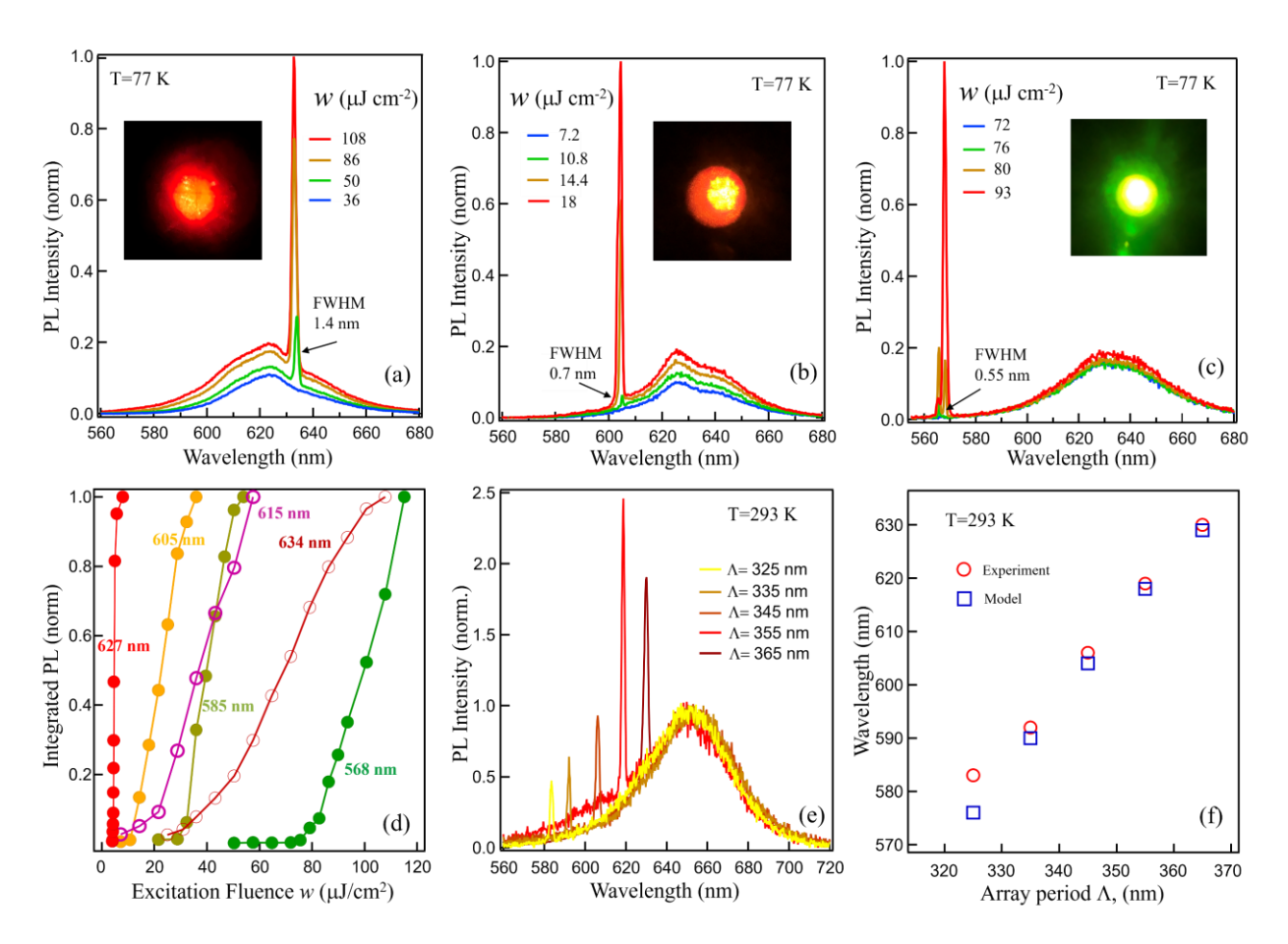


Figure 4. (a-c) Lasing emission lines measured at T=77 K for various array periods Λ . (a) Λ =365 nm, (b) Λ =335 nm, (c) Λ =315 nm. Insets: Microphotographs of the lasing spots. (d) Lasing thresholds as a function of excitation fluence for different lasing lines. (e) Lasing emission lines measured at T=293 K. (f) Calculated (blue) νs . experimental (red) positions of the lowest energy resonance/lasing peaks as a function of the nanopillar array periods for T=293 K.

attributed to variance in QS depositions within each array, as shown in **Figure 4f**. Simulated transmission resonances for all array periods are shown in **Figure S7**.

We examined the emergence of lasing lines alongside the evolution of the optical gain band, as determined by femtosecond transient absorption (TA) spectroscopy. **Figure 5a** presents TA transmission spectrum for QS solution at room temperature. However, obtaining a similar TA spectrum for the QS/nanopillar sample was unfeasible due to experimental limitations. Taking into consideration the low-temp bandgap renormalization, the figure reveals BX optical gain (absorption α <0) at lower excitation fluence, which evolves into higher energy gain associated

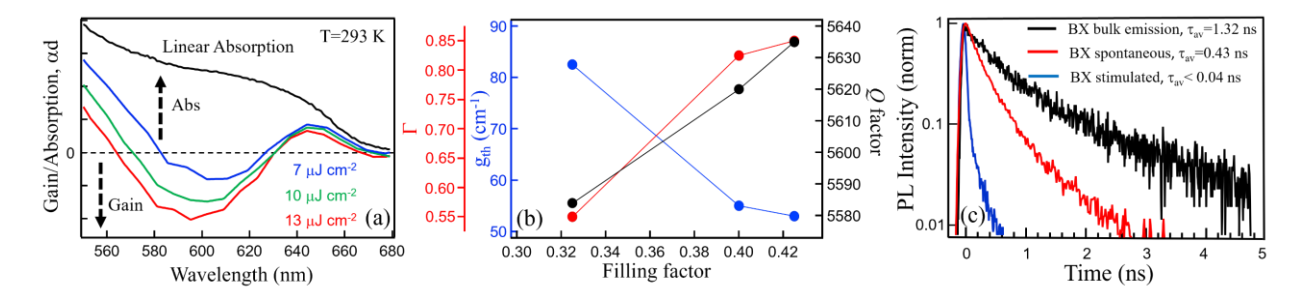


Figure 5. (a) Room temperature TA spectra for 6-nm core QSs in solution at various excitation fluences. Positive values indicate absorption, negative – optical gain. (b) Threshold gain, confinement factor and *Q* factor as a function of the filling factor. (c) PL lifetimes for QSs at BX transition. Black trace – spontaneous emission outside of nanopillar array, red trace - spontaneous emission inside the array, blue trace – stimulated emission inside the array.

with excited state BXs at 1S(e)-2S(h) and MX 1P(e)-1P(h) interband transitions. A more comprehensive discussion of the TA spectroscopy methodology can be found in the SI section. The appearance of lasing lines clearly follows the spectral gain evolution, with lowest threshold BX emission appearing near the minimum of TA gain and followed by laser lines with larger excitation thresholds at the higher energies. The mode confinement factor and its corresponding threshold gain can be calculated with the following formula⁴⁵, $g_{th} = \frac{n_{CdSe}*\omega_0}{c*\Gamma*Q}$ (cm^{-1}), where ω_0

is the modal frequency. $\Gamma = \frac{W_{e,a}}{W_{e,tot}}$ is the mode confinement factor, where $W_{e,a}$ is the electric field energy in the active medium and $W_{e,tot}$ is the electric field energy everywhere. Figure 5b shows a theoretical threshold gain as function of the filling factor, with values around g_{th} = 40 ~ 80 cm⁻² ¹ for the nanopillar array with Λ =345 nm. The values for other arrays are similar, **Figure S8**. As the gain material filling factor (inverse with respect to SiO₂ nanopillar diameter) decreases, the mode becomes less confined, resulting in a decreased Q factor and larger threshold gain. The Q factors are calculated by Fano fitting the guided resonances in transmission spectra, 46,47 and the cavity Q factors of several Fano resonances near the lasing emission wavelength are around $Q \sim$ 6,000. Since we assumed an infinite number of periods in the simulation, only radiation loss was considered. Experimentally, the Q factor can be estimated with $Q = \lambda_0 / \delta \lambda$, where λ_0 is the resonant wavelength ($\lambda_0 = 2\pi c/\omega_0$) and $\delta\lambda$ is the FWHM of the lasing mode. The narrowest linewidth for the BX transition is $\delta\lambda \sim 0.5$ nm, rendering $Q \sim 1200$ and $g_{th} \sim 200 \sim 400$ cm⁻¹. These values are comparable to or smaller than ASE modal gain values measured for the thin film configuration without cavity, Figure 1c, underlying the advantage of the cavity. The Purcell enhancement factor $F = \Gamma_{cav}/\Gamma_0$, where Γ_{cav} is the enhanced spontaneous emission rate into the cavity mode and Γ_0 is the rate in the absence of the cavity (free space or bulk). Therefore, when the spontaneous emission rate is enhanced (F>1) and emission into non-cavity modes is suppressed, most of the emission is channeled into the lasing mode, resulting in the reduction of the lasing threshold. To independently measure the Purcell factor, we recorded the PL emission lifetime for BX emission line under spontaneous emission conditions at low fluence, Figure 5c. Black trace represents lifetime for QSs away from the nanopillar array (i.e. bulk emission), while the red one is for QSs inside the array. Both lifetimes can be fitted with double exponential decays, with contributions likely arising from various degrees of electronic and excitonic coupling within thick QS layer. 48,49 Nevertheless,

following standard routine, we computed averaged emission lifetime of a biexponential function as τ_{av} =($A_1*\tau_1^2 + A_2*\tau_2^2$)/($A_1*\tau_1 + A_2*\tau_2$) where A_i is an amplitude and τ_i is the lifetime of a given component. We obtained $\tau_{av} \sim 1.32$ ns for the BX bulk emission and $\tau_{av} \sim 0.43$ ns for the spontaneous BX emission inside the array, rendering Purcell factor F~3.1. Upon increasing the excitation fluence above the lasing threshold, the BX lifetime transitions into the stimulated emission regime with resolution-limited τ_{stim} < 40 ps, blue trace on **Figure 5c**. Analogously, the threshold excitation fluence reduces from $w \sim 10 \ \mu J/cm^2$ for planar-type, ASE waveguiding mode of the thin film to $w \sim 4 \ \mu J/cm^2$ for the PhC array.

Conclusions:

In summary, our study successfully demonstrates lasing from colloidal quantum shells employing nanopillar photonic crystal cavities. This investigation validates the superior material gain of QS geometry, surpassing performance levels typically associated with colloidal quantum dots. In particular, we achieve near-record performance in lowering the lasing threshold of solution-processed lasers and extending the spectral range of amplified emission through accessing population inversion in multi-exciton states. The suppression of Auger recombination and reduction of optical losses within the PhC cavity are the critical factors contributing to these outcomes. Overall, this work underscores the compelling potential of colloidal QSs for the development of practical, scalable, and efficient lasers, suitable for a wide range of photonic applications.

Acknowledgement. This work was supported by the U.S. Department of Energy, Office of Science under the contract DE-SC0010697. The work of the BGSU team was supported by the award DE-

SC0016872 (MZ). DH and MZ acknowledge the support by NSF award #2208834. Qing Gu acknowledges the support by NSF CAREER award ECCS-2209871.

Supporting Information. QS synthesis, fabrication of nanopillar arrays, calculations of absorption cross-section. Available free of charge at https://pubs.acs.org/doi

References

_

¹ Roelkens, G., Van Campenhout, J., Brouckaert, J., van Thourhout, D., Baets, R., Romeo, P. R., Regreny, P., Kazmierczak, A., Seassal, C., Letarte, X, et al, III-V/Si Photonics by Die-to-Wafer Bonding, *Mater. Today* **2007**, *10*, 36-43

² Krishnamoorthy, A. V., Goossen, K. W., Optoelectronic-VLSI: Photonics Integrated with VLSI Circuits, *IEEE J. Sel. Top. Quantum Electron.* **1998**, *4*, 899-912

³ Orieux, A., Diamanti, E., Recent Advances on Integrated Quantum Communications. *J. Opt.* **2016**, *18*, 083002

⁴ Higurashi, E., Sawada, R., Ito, T., An Integrated Laser Blood Flowmeter, *J. Light. Technol.* **2003**, *21*, 591

⁵ Vannahme, C., Klinkhammer, S., Lemmer, U., Mappes, T., Plastic Lab-on-a-Chip for Fluorescence Excitation with Integrated Organic Semiconductor Lasers, *Opt. Express* **2011**, *19*, 8179-8186

⁶ Ahn, N., Livache, C., Pinchetti, V., Klimov, V. I., Colloidal Semiconductor Nanocrystal Lasers and Laser Diodes, *Chem. Rev.* **2023**, *123*, 8251-8296

⁷ Klimov, V. I., Mikhailovsky, A. A., Xu, S., Malko, A., Hollingsworth, J.A., Leatherdale, C. A., Eisler, H. J., Bawendi, M. G., Optical Gain and Stimulated Emission in Nanocrystal Quantum Dots, *Science*, **2000**, *290*, 314-317

⁸ Wang, Y., Sun, H., Advances and Prospects of Lasers Developed from Colloidal Semiconductor Nanostructures, *Prog. Quantum Electron.* **2018**, *60*, 1-29

⁹ Geiregat, P., van Thournhout, D. Hens, Z., Bright Future for Colloidal Quantum Dot Lasers, *NPG Asia Mater.*, **2019**, *11*, 41

¹⁰ Kwak, J., Lim, J., Park, M., Lee, S., Char, K., Lee, C., High-Power Genuine Ultraviolet Light-Emitting Diodes Based on Colloidal Nanocrystal Quantum Dots, *Nano Lett.*, **2015**, *15*, 3793-3799

¹¹ Pradhan, S., Dalmases, M., Taghipour, N., Kundu, B., Konstantanos, G., Colloidal Quantum Dot Light Emitting Diodes at Telecom Wavelength with 18% Quantum Efficiency and Over 1 MHz Bandwidth, *Adv. Sci.* **2022**, *9*, 2200637

¹² Murray, C. B., Norris, D. J., Bawendi, M. G., Synthesis and Characterization if Nearly Monodisperse CdE (E=Sulfur, Selenium, Tellurium) Semiconductor Nanocrystallites, *J. Am. Chem. Soc.* **1993**, *115*, 8706-8715

¹³ Peng, X. G., Manna, L., Yang, W. D., Wickham, J., Scher, E., Kadavanich, A., Alivisatos, A. P., Shape Control of CdSe Nanocrystals, *Nature* **2000**, *404*, 59-61

- ¹⁴ Son, J.S., Yu, J. H., Kwon, S. G., Lee, J., Joo, J., Hyeon, T., Colloidal Synthesis of Ultrathin Twi-Dimensional Semiconductor Nanocrystals, *Adv. Mater.* **2011**, *23*, 3214-3219
- ¹⁵ Ithurria, S., Tessier, M. D., Mahler, B., Lobo, R. P. S. M., Dubertret, B., Efros, A. L., Colloidal Nanoplatelets with Two-Dimensional Electronic Structure, *Nat. Mater.* **2011**, *122*, 12700-12706
- ¹⁶ Klimov, V. I., Mikhailovsky, A. A., McBranch, D. W., Leatherdale, C. A. & Bawendi, M. G. Quantization of Multiparticle Auger Rates in Semiconductor Quantum Dots. *Science* **2000**, 287, 1011–1013
- ¹⁷ Bae, W. K., Park, Y.-S., Lim, J., Lee, D., Padilha, L. A., McDaniel, H., Robel, I., Lee, C., Pietryga, J. M. & Klimov, V. I. Controlling the Influence of Auger Recombination on the Performance of Quantum-Dot Light-Emitting Diodes. *Nat. Comm.* **2013**, 4, 2661
- ¹⁸ Bae, W. K., Padilha, L. A., Park, Y.-S., McDaniel, H., Robel, I., Pietryga, J. M., Klimov, V. I., Controlled Alloying of the Core-Shell Interface in CdSe/CdS Quantum Dots for Suppression of Auger Recombination, ACS Nano, 2013, 7, 3411-3419
- ¹⁹ Park, Y.-S., Lim, J., Makarov, N. S., Klimov, V. I., Effect of Interfacial Alloying versus "Volume Scaling" on Auger Recombination in Compositionally Graded Semiconductor Quantum Dots, Nano Lett., 2017, 17,5607-5613
- ²⁰ Ma, X.; Diroll, B. T.; Cho, W.; Fedin, I.; Schaller, R.D.; Talapin, D. V.; Gray, S. K.; Wiederrecht, G. P.; Gosztola, D. J. Size-Dependent Biexciton Quantum Yields and Carrier Dynamics of Quasi-Two-Dimensional Core/Shell Nanoplatelets. *ACS Nano* **2017**, 11, 9119-9127
- ²¹ Fan, F., Voznyy, O., Sabatini, R. P., Bicanic, K. T., Adachi, M. M., McBride, J. R., Reid, K. R., Park, Y.- S., Li, X., Jain, A., Quintero-Bermidez, R., Saravanapavanantham, S., Liu, M., Korkusinski, M., Hawrylak, P., Klimov, V. I., Rosenthal, S. J., Hoogland, S., Sargent, E. H., Continuous-Wave Lasing in Colloidal Quantum Dot Solids Enabled by Facet-Selective Epitaxy, *Nature*, **2017**, *544*, 75-79.
- ²² Lim, J., Park, Y.-S., Klimov, V. I., Optical Gain in Colloidal Quantum Dots Achieved with Direct-Current Electrical Pumping, *Nat. Mater.* **2018**, *17*, 42-49
- ²³ Ahn, N., Livache, C., Pinchetti, V., Jung. H., Jin. H., Hahm, D., Park, Y.-S., Klimov, V.I., Electrically Driven Amplified Spontaneous Emission from Colloidal Quantum Dots, *Nature*, **2023**, *617*, 79-85
- ²⁴ Rashba, E. I., Giant Oscillator Strengths Associated with Exciton Complexes. *Sov. Phys. Semicond.* **1975**, 8, 807-816
- ²⁵ Rowland, C. E., Fedin, I., Zhang, H., Gray, S. K., Govorov, A. O., Talapin, D. V., Schaller, R. D., Picosecond Energy Transfer and Multiexciton Transfer Outpaces Auger Recombination in Binary CdSe Nanoplatelet Solids, *Nat. Mater.* **2015**, *14*, 484-489
- ²⁶ N. Razgoniaeva, P. Moroz, M. Yang, D. S. Budkina, H. Eckard, M. Augspurger, D. Khon, A. N. Tarnovsky, M. Zamkov, One-Dimensional Carrier Confinement in "Giant" CdS/CdSe Excitonic Nanoshells, *J. Am. Chem. Soc.*, 2017, **139**, 7815–7822.

²⁷ N. Kholmicheva, D. S. Budkina, J. Cassidy, D. Porotnikov, D. Harankahage, A. Boddy, M. Galindo, D. Khon, A. N. Tarnovsky and M. Zamkov, Sustained Biexcitonic Populations in Nanoshell Quantum Dots, *ACS Photonics*, 2019, **6**, 1041–1050.

- ²⁸ G. Nagamine, B. G. Jeong, T. A. C. Ferreira, J. H. Chang, K. Park, D. C. Lee, W. K. Bae and L. A. Padilha, Efficient Optical Gain in Spherical Quantum Wells Enabled by Engineering Biexciton Interactions, *ACS Photonics*, 2020, **7**, 2252–2264.
- ²⁹ J. Cassidy, B. T. Diroll, N. Mondal, D. B. Berkinsky, K. Zhao, D. Harankahage, D. Porotnikov, R. Gately, D. Khon, A. Proppe, M. G. Bawendi, R. D. Schaller, A. V. Malko and M. Zamkov, Quantum Shell Boost the Optical Gain of Lasing Media, *ACS Nano*, 2022, **16**, 3017–3026.
- ³⁰ A. H. Proppe, K. L. K. Lee, C. L. Cortes, M. Saif, D. B. Berkinsky, T. Sverko, W. Sun, J. Cassidy, M. Zamkov, T. Kim, E. Jang, S. K. Gray, B. A. McGuire and M. G. Bawendi, Adversarial autoencoder ensemble for fast and probabilistic reconstructions of few-shot photon correlation functions for solid-state quantum emitters *Phys. Rev. B*, 2022, **106**, 045425.
- ³¹ J. Cassidy, D. Harankahage, D. Porotnikov, A. V. Malko and M. Zamkov, Colloidal Quantum Shells: An Emerging 2D Semiconductor for Energy Applications, *ACS Energy Lett.*, 2022, 7, 1202–1213.
- ³² Harankahage, D., Cassidy, J., Beavon, J., Huang, J., Brown, N., Berkinsky, D., Zhang, K., Anzenbacher, P., Schaller, R., Sun, L., Bawendi, M., Malko, A., Diroll, B., Zamkov. M. Quantum Shell in a Shell: Engineering Colloidal Nanocrystals for a High-Intensity Excitation Regime, *J. Am. Chem. Soc.*, **2023** *145*, 13326–13334.
- ³³ Marder, A. A., Cassidy, J., Harankahage, D., Beavon, J., Gutierrez-Arzaluz, L., Mohammed, O. F., Misra, A., Adams, A. C., Slinker, J. D., Hu, Z., Savoy, S., Zamkov M., Malko, A. V., CdS/CdSe/CdS Spherical Quantum Wells with Near-Unity Biexciton Quantum Yield for Light-Emitting Device Applications, *ACS Materials Lett.* **2023**, *5*, 1411–1419
- ³⁴ A. Malko, A. Mikhailovsky, M. Petruska, J. Hollingsworth, H. Htoon, M. Bawendi, and V. Klimov, From amplified spontaneous emission to microring lasing using nanocrystal quantum dot solids, *Appl. Phys. Lett.* **2002**, *81*, 1303.
- ³⁵ Wang Y, Ta V D, Leck K S, et al. Robust whispering-gallery-mode microbubble lasers from colloidal quantum dots, *Nano Lett*, **2017**, *17*, 2640–2646
- ³⁶ Guzelturk, B., Kelestemur, Y., Olutas, M., Delikanli, S., Demir, H. V. Amplified spontaneous emission and lasing in colloidal nanoplatelets. *ACS Nano* **2014**, *8*, 6599–6605.
- ³⁷ Dang, C. et al. Red, green and blue lasing enabled by single-exciton gain in colloidal quantum dot films. *Nat. Nanotechnol.* **2012**, *7*, 335–339
- ³⁸ Kozlov, O. V.; Park, Y.-S.; Roh, J.; Fedin, I.; Nakotte, T.; Klimov, V.I.; Sub-Single-Exciton Lasing Using Charged Quantum Dots Coupled to a Distributed Feedback Cavity. *Science* **2019**, *365*, 672-675
- ³⁹ Roh, J., Park, Y.-S., Lim, J., Klimov, V. I., Optically Pumped Colloidal-Quantum-Dot Lasing in LED-like devices with an Integrated Optical Cavity, *Nat. Comm.*, **2020**, *11*, 271.
- ⁴⁰ Painter, O, Lee, R. K., Scherer, A., Yariv, A., O'Brien, J. D., Dapkus, P. D., Kim, I., Two-dimensional photonic band-gap defect mode laser. *Science* **1999**, 284, 1819-1821.

⁴¹ Wu, S, Buckley, S., Schaibley, J. R., Feng, L., Yan, J, Mandrus, D. G., Hatami, F., Yao, W., Vuckovic, J., Majumdar, A., Xu, X, Monolayer semiconductor nanocavity lasers with ultralow

thresholds, *Nature* **2015**, 520, 69-72.

⁴² Moon, J., Alahbakhshi, M., Gharajeh, A., Li, Q., Li, Z., Haroldson, R., Kwon, S., Hawkins, R., Kim, M. J., Hu, W., Zhang, X., Zakhidov, A., Gu, Q, Quasi-CW lasing from directly patterned and encapsulated perovskite cavity at 260 K, *ACS Photonics* **2022**, 9, 984-1991.

- ⁴³ Park, Y.-S., Rph, J., Diroll, B. T., Schaller, R. D., Klimov, V. I., Colloidal Quantum Dot Lasers, *Nature* **2021**, *6*, 382
- ⁴⁴ Chen, M., Lu, L., Yu, H., Li, C., Zhao, N., Integration of Colloidal Quantum Dots with Photonic Structures for Optoelectronic and Optical Devices, *Adv. Sci.* **2021**, *8*, 2101560
- ⁴⁵ Li, Z., Moon, J., Gharajeh, A., Haroldson, R., Hawkins, R., Hu, W., Zakhidov, A., Gu, Q., Room-Temperature Continuous-Wave Operation of Organometal Halide Perovskite Lasers, *ACS Nano* **2018**, *12*, 10968–10976
- ⁴⁶ Limonov, M. F., Rybin, M. V., Poddubny, A. N., Kivshar, Y. S., Fano resonances in photonics, *Nat. Photon.* **2017**, *11*, 543-554
- ⁴⁷ Limonov, M. F., Fano resonance for applications, Adv. Opt. Photonics **2021**, 13, 703-771
- ⁴⁸ Franzl, T., Klar, T. A., Schietinger, S., Rogach, A. L., Feldmann, J., Exciton recycling in graded gap layer-by-layer semiconductor nanocrystal structures, *Nano Lett.* **2004**, *4*, 1599.
- ⁴⁹ Rupich, S. M., Gartstein, Y. N., Chabal Y. J., Malko, A.V. Controlled Deposition of High-Quality Nanocrystal Multilayers Structures for Optoelectronic Applications, *Adv. Opt. Mat.*, **2016**, *4*, 378-383
- 50 Lakowicz, J. R., Principles of Fluorescence Spectroscopy, $3^{\rm rd}$ edition, **2006**, 10.1007/978-0-387-46312-4.